IEEE Photonics Journal
An IEEE Photonics Society Publication

Silicon Photomultipliers for Deep Tissue Cerenkov Emission Detection During External Beam Radiotherapy

Volume 11, Number 4, August 2019

Ibrahim Oraiqat
Samuel DeBruin
Robin Pearce
Christopher Como
Justin Mikell
Charles Taylor
John Way
Manuel Suarez
Alnawaz Rehemtulla
Roy Clarke
Issam El Naqa, *Senior Member, IEEE*

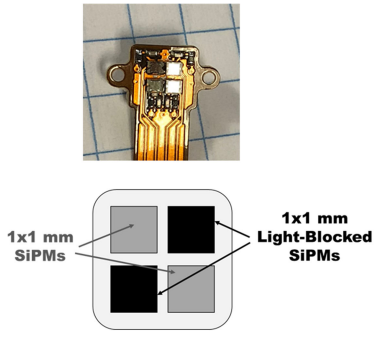

Depth (mm)	SiPM Signal (mV)	Photodiode Signal (mV)	Ratio (SiPM/PD)
1	944 ± 4	7.5 ± 0.2	126
5	490 ± 6	0.8 ± 0.1	612
7	364 ± 5	0.3 ± 0.1	1,213
35	24 ± 3	-	-

DOI: 10.1109/JPHOT.2019.2931845

Silicon Photomultipliers for Deep Tissue Cerenkov Emission Detection During External Beam Radiotherapy

Ibrahim Oraiqat,[1] Samuel DeBruin,[2] Robin Pearce,[3] Christopher Como,[3] Justin Mikell,[1] Charles Taylor,[3] John Way,[3] Manuel Suarez,[3] Alnawaz Rehemtulla,[1] Roy Clarke,[2,4] and Issam El Naqa,[1] *Senior Member, IEEE*

[1]Radiation Oncology Department, University of Michigan, Ann Arbor, MI 48109 USA
[2]Endectra, LLC, Ann Arbor, MI 48109 USA
[3]Biomedical Engineering Department, University of Michigan, Ann Arbor, MI 48108 USA
[4]Physics Department, University of Michigan, Ann Arbor, MI 48109 USA

DOI:10.1109/JPHOT.2019.2931845

Manuscript received June 5, 2019; revised July 22, 2019; accepted July 24, 2019. Date of publication July 29, 2019; date of current version August 13, 2019. This work was supported by NIH grant R37CA222215 and Endectra, LLC (NSF SBIR Phase II #1632467). Corresponding author: Ibrahim Oraiqat (e-mail: ioraiqat@umich.edu).

Abstract: Cerenkov Emission (CE) during external beam radiation therapy (EBRT) from a linear accelerator (Linac) has been demonstrated as a useful tool for radiotherapy quality assurance and potentially other applications for online tracking of tumors during treatment delivery. However, some of the current challenges that are impacting the potential of CE are related to the limited detection sensitivity and the lack of flexible tools to fit into an already complex treatment delivery environment. Silicon photomultiplier (SiPM) solid-state devices are new promising tools for low light detection due to their extreme sensitivity that mirrors photomultiplier tubes and yet have a form factor that is similar to silicon photodiodes, allowing for improved flexibility in device design that may help in the process of wider clinical applicability. In this paper, we assess the feasibility of using SiPMs to detect CE during EBRT from a Linac and contrast their performance with commercially available silicon photodiodes (PDs). We demonstrate the feasibility of the SiPM-based probes for standard dosimetry measurements. We also demonstrate that CE optical signals can be detected from tissue depths about five times greater than that for standard probes based on PDs, making our SiPM probe an enabling technology of CE measurements, particularly for deep tissue applications.

Index Terms: Radiotherapy, Biophotonics Instrumentation, Cerenkov emission, Silicon photomultiplier, Medical photonics instrumentation.

1. Introduction

Radiotherapy is widely used in the treatment of malignant tumors with more than 60% of all cancer patients receiving ionizing radiation as a main part of their treatment [1]. It is recognized that the efficacy of radiation treatment is highly dependent on the accurate delivery of radiation dose up to the lesion boundary. Currently, evaluating the efficacy of radiation treatment is generally an offline process where radiation technologists use added margins during the planning process and make setup adjustments based on cone beam computed tomography (CBCT), just prior to delivery of high levels of ionizing radiation. The use of added margins is to account for inaccuracies in patient placement on the treatment table and internal organ motion uncertainties, thus exposing both

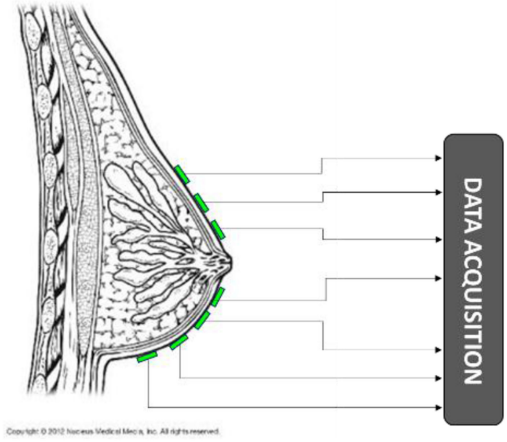

Fig. 1. A proposed schematic of placing multiple SiPM optical probes directly onto a breast for in vivo dosimetric point measurements using CE.

heterogeneous cancerous and non-cancerous tissues in parallel to high energy ionizing radiation. This also inadvertently results in inefficient tumor cell kill and increased exposure of surrounding vital normal tissue causing inflammatory reactions and other detrimental radiation-related side effects. Therefore, methods for detecting radiation during delivery (i.e., *in vivo* dosimetry) are needed to improve targeting accuracy and reduce radiation-induced side effects.

The induction of an intrinsic, optical emission signal during irradiation treatment, known as Cerenkov Emission (CE) has been shown to be detectable during external beam radiotherapy (EBRT) delivery by clinical linear accelerators (Linacs) [2]–[5]. CE is generated as visible light when charged particles (in this case, secondary electrons) travelling at speeds larger than the phase velocity, v_p, of light polarize the medium along its track by energy transfer to the surrounding molecules through Coulombic interactions. Subsequently, the electric dipoles created in the medium are de-excited by photon emission. If the particle speed is larger than v_p, the polarization becomes asymmetric along the particle track because dipoles de-excite more slowly than they are created [6]. CE has a characteristic spectrum whereby the intensity of the light produced is inversely proportional to the wave length, i.e., primarily in the blue and ultraviolet (UV) part of the electromagnetic spectrum; this results in a low photon count through human tissue due to absorption by hemoglobin circulating the blood, skin melanin, and bilirubin [7], [8].

Although CE is well known in the field of radiation physics, its exploitation in cancer imaging is only beginning to be realized recently. It has been investigated for potential applications in radiation dosimetry [2], [9]–[11] and tracking during radiotherapy [12], using superficial (1–2 mm deep) CE measurements to map radiation dose from Linacs. However, CE measurements from deep tissue (for example, within the breast) is currently limited by the combination of the sensitivity of current photo-detectors, which are mainly based on complementary metal–oxide–semiconductor (CMOS) or charge-coupled devices (CCDs) as well as inverse square losses of CE optical photons when using a camera to image from a distance. To address these limitations, we propose to use a flexible and effective approach based upon a novel design of on-body optical probes incorporating extremely sensitive Silicon Photomultipliers (SiPMs) to map the delivered dose by radiotherapy in real time (see Fig. 1). Placing the optical probes directly onto the surface mitigates the optical inverse square losses, making this approach more suitable for deep tissue measurements, where very few optical photons are leaving the surface. These types of probes can easily be integrated into patient positioning and immobilization devices (such as radiation treatment brassieres that are used to conform the breast to a reproducible shape) and to reduce set up complexities.

Important advantages of SiPMs include their superior response in the blue range of the electromagnetic spectrum and their well-known extreme sensitivity, similar to a conventional photomultiplier tube; these characteristics can enable SiPMs quantify low-level CE signals down to the

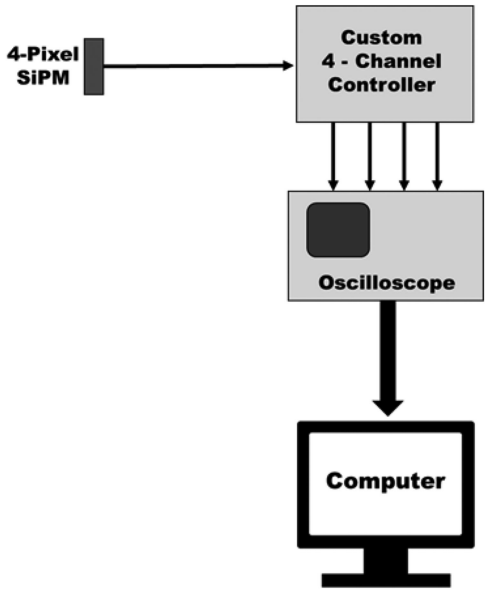

Fig. 2. Data acquisition schematic for the prototype SiPM optical probe system.

single-photon level. These SiPM devices are built from an avalanche photodiode (APD) array with different quenching resistors printed onto a common silicon substrate [13]. Unlike CCDs, SiPMs can be read in parallel like CMOS but with much higher sensitivity, which makes them an attractive choice for recent medical imaging detector applications such as Single Photon Emission Computer Tomography (SPECT) and Positron Emission Tomography (PET) [14], [15]. SiPMs have also recently been used for both continuous and time domain optical measurements [16], [17]. Ferocino, *et al.*, have recently built a SiPM-based 8-channel detection chain for time domain optical mammography to improve the signal level and system robustness (to bring it into the clinic) [18]. Related to our work, improved imaging of CE from internally injected radioisotopes ($\beta+$ emitters) was demonstrated using SiPM-based detectors, compared to standard CMOS/CCD cameras [19], [20]. In addition, Mouthino *et al.*, reported the design of a low-dose rate brachytherapy dosimeter using a scintillating fiber optic coupled to a SiPM [21].

In this paper, we focus on introducing our design for capturing useful CE signals during EBRT. This design uses a custom multi-channel SiPM-based optical probe for CE measurements that may be placed on the skin during EBRT. We first describe the overall design of the probe and then characterize the performance of the SiPM-based optical probe for dosimetry measurements in a water tank. This is followed by a comparison with a silicon photodiode (PD) probe for detecting optical signals deep inside tissue (ground pork is used for this comparison). Note that in this case the CE signal falls mostly outside of the near infrared biological optical window (650 nm-900 nm) [22], and thus constitutes a challenging test to demonstrate the potential of using SiPMs for deep tissue CE optical measurements.

2. Materials and Methods

2.1 SiPM Design for External Beam Radiotherapy Applications

The 4 mm^2 (active area) probe is designed around four 1 mm $\times$ 1 mm SiPMs (SensL MicroFC-10035-SMT) pixels. Each pixel corresponds to a single channel. The probe itself is mounted onto a flexible substrate that allows the probe and the flexible connector (which supplies power to the probe and carries the signal from each SiPM pixel) to act as an integrated and flexible single device. Having a flexible substrate would also allow multiple probes to conform properly to arbitrary tissue

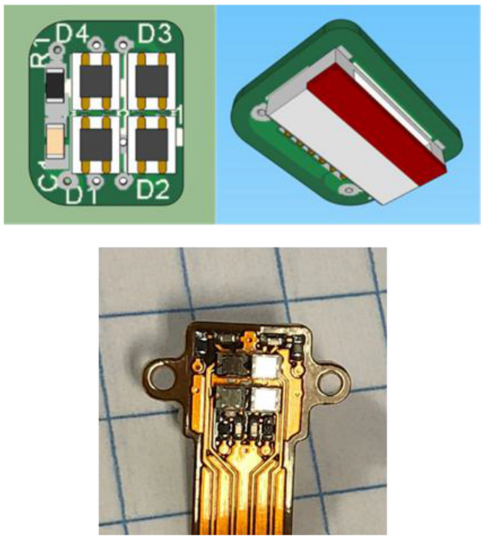

Fig. 3. Top: Technical drawing of the front and back of the SiPM probe. Bottom: A photograph of the SiPM probe showing its small size (note: grid lines in the background are 6 × 6 mm).

shapes (e.g., in the breast case as shown in Fig. 1 or other body tissues in case of head and neck or lymphomas). The overall dimensions of the probe region are 6 mm wide, 5 mm long, and 1.5 mm thick. The flexible cable is 3.7 mm wide and can be up to 25 cm long. At the other end of the flexible cable is the controller, which generates power for the probe and amplifies the return signals. Fig. 3 (top-left) represents the top view of the probe, showing the four SiPM pixels and the supply biasing components. Fig. 3 (top-right) shows a view of the bottom of the probe, showing the opening to the flat-flexible connector housing. The bottom of Fig. 3 is a photograph of the probe, showing the probe and cable are a single, flexible unit. The four pixels on the probe are negatively biased at approximately −29 V. The bias voltage is configurable through a custom-made controller circuit to adjust for specific conditions. The probe itself contains conditioning circuitry for the bias voltage. The four signals from the probe are DC-coupled to the controller, which contains an integrated transimpedance amplifier with a nominal amplification of 2200 V/A.

Fig. 4 shows the SiPM pixel arrangement. Two SiPM pixels are covered in light blocking material while the other two are left as open pixels for light detection. The reason for this is to distinguish optical signals from scattered x-ray signals and stem effects (i.e., CE induced in any extra material on top of the SiPM, such as a transparent plastic wrap to act as a biological barrier between the probe and phantom). Data acquisition is gated to the Linac target trigger and signals from all four channels are collected simultaneously using an oscilloscope (GW Instek GDS-3504); this collected signal corresponds to a single Linac pulse. The oscilloscope transfers data to a computer for further processing (as shown in Fig. 2). The difference is taken between one open pixel and an adjacent light-blocked pixel. This difference yields the optical signal that is purely from the CE of the phantom during a single Linac pulse, removing any signals that result from direct x-rays and signals that may result from CE generated in any media associated with the probe (i.e., background stem effect). The choice of which adjacent pixel is light-blocked depends on the geometry of the measurement. For example, if measurements are taken horizontally (such as looking at a horizontal gradient of CE intensity), the adjacent light-blocked blocked pixel should be vertically oriented relative to the open light detection pixel, thus keeping them on the same plane with respect to the signal gradient.

For all measurements, the entire set-up (including phantoms) is wrapped in a light blocking fabric (ThorLabs BK5 black rubberized plastic) and the treatment room lights are turned off to reduce any background optical signals. Data acquisition is gated to individual Linac pulses by triggering the oscilloscope to the target output (which is the current generated when electrons strike the tungsten target to produce 6 MV x-rays) of the Linac. Each trace is an average of 32 traces

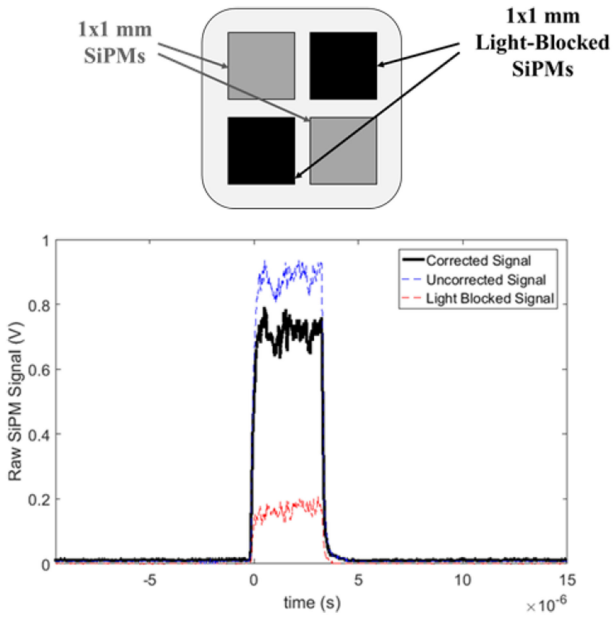

Fig. 4. Top: Schematic of SiPM pixel arrangement, showing two channels that are blocked out to optical light to aid distinguish optical signals from scattered x-ray signals and background correction. Bottom: An example data trace showing the uncorrected signal, the light blocked signal, and the corrected signal.

from individual Linac pulses. The amplitude is measured during post-processing and a total of 10 amplitude measurements are collected and averaged. All data for subsequent experiments, unless otherwise noted, are acquired in this fashion. The treatment room temperature is controlled using the HVAC thermostat, the temperature was 69 $\pm$ 1 °F for the duration of the experiments.

2.2 CE Dosimetry in Water Using the SiPM Probe

CE was stimulated using 6 MV photon beam generated in a Linac (Varian TrueBeam) and measured using the SiPM probes that are gated to the Linac target trigger. Instantaneous dose is defined here as the dose delivered during an individual Linac pulse. The signal pulse height (in V) from the SiPM probe is proportional to the intensity of CE during that pulse, which is in turn proportional to dose.

Initially, measurements of CE intensity versus depth inside a water tank were taken to generate percent depth dose (PDD) curves using the SiPM optical probes at 6 MV. The water tank is setup at 100 cm Source to Surface Distance (SSD). As a reference, SiPM measurements are compared to ion chamber PDD measurements in a water tank that were acquired at 100 cm SSD during the linac commissioning. In order to spatially localize CE, a light collimator is used since the probe signal is an integration of all of the CE within the solid angle of acceptance of the probe, hence reduction this solid angle of acceptance would improve the probe's spatial resolution. The light collimator, which consists of a black hollow tube with a length of 22.5 mm and an inner diameter of 4.15 mm, is attached to the SiPM probe to reduce the solid angle of detection for the probe from 2π steradian to approximately 0.006π steradian, as seen in Fig. 5. The edge of a 3 $\times$ 3 cm radiation field is placed 9 mm from the surface of the collimator of the SiPM probe and 4 mm from the tank surface; depth, z, is measured from the center of the top two pixels of the probe to the water surface, as shown schematically in Fig. 6. The probe pixel for light collection (i.e., not blacked out) is aligned to the center of the field. The probe position is adjusted by using a motorized translation stage (Thorlabs MTS50-Z8) controlled from the treatment room. The depth range is measured from 0 mm to 80 mm,

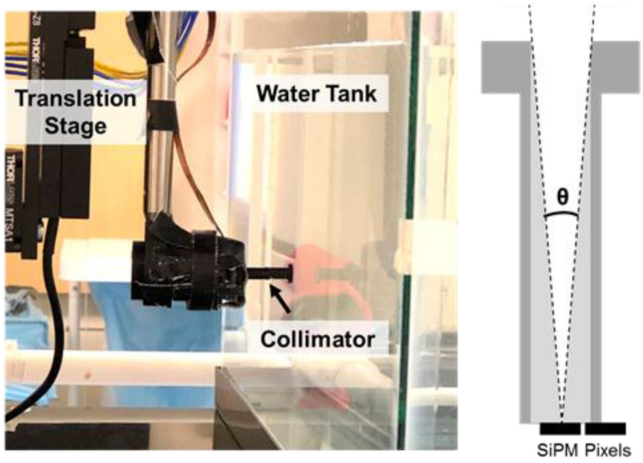

Fig. 5. Left: SiPM attached to the translation stage for water tank PDD measurements. Right: Schematic of the collimator setup, to reduce the solid angle of detection to 0.006π steradian.

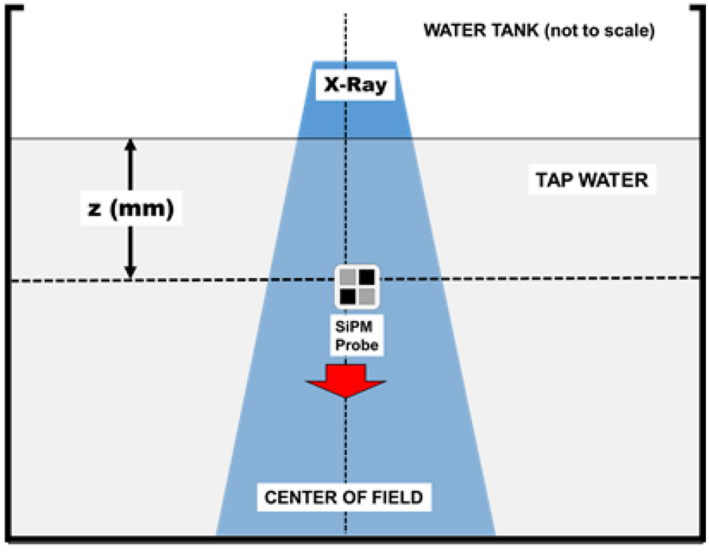

Fig. 6. Schematic of the PDD experimental setup with the collimator facing into the Figure and the light collecting pixel aligned to the center of the field.

with 2.5 mm intervals until a depth of 20 mm, followed by an interval of 5 mm until 40 mm, followed by an interval of 10 mm until 80 mm.

Due to the divergence of the radiation beam, the distance between the surface of the probe collimator and the edge of the field's distance varies with depth (as shown in Fig. 7) since the probe's distance to the tank surface is held constant; therefore, a correction factor as a function of the tank depth is applied for each depth point using similar triangles and the inverse-square law. This correction factor gives the intensity value as if the source was positioned at isocenter.

The intensity is adjusted using the equation:

$$I_{adjusted} = I_{raw} \frac{d_n^2}{d_0^2} \tag{1}$$

Where $I_{adjusted}$ is the corrected intensity signal, I_{raw} is the measured intensity at each depth point. As shown in Fig. 7, d_0 is the initial distance between the edge of the field and the collimator surface (e.g., at isocenter), and d_n is the distance between the edge of the field and the collimator surface

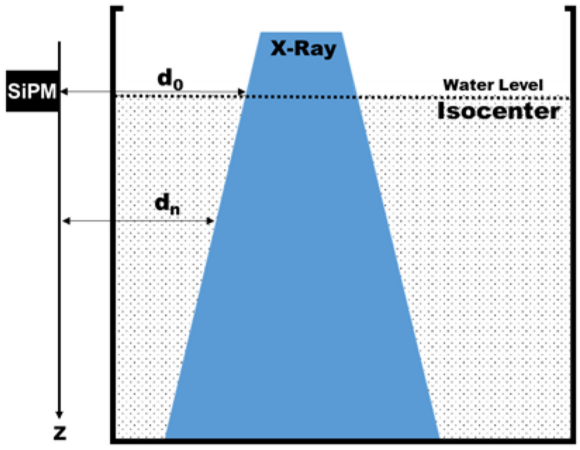

Fig. 7. Side view of the experimental setup. The probes are aligned so they are at a constant depth from the water surface (10 cm).

at each depth, which is defined as:

$$d_n = d_0 - \left[\frac{1}{2}\left(FieldWidth_n - FieldWidth_0\right)\right] \tag{2}$$

Where $FieldWidth_0$ is the field-width in the direction normal to the SiPM probe at isocenter and $FieldWidth_n$ is the field-width at subsequent depths, which changes (using similar triangles) as:

$$FieldWidth_n\ (in\ mm) = \frac{(1000\ +\ z)}{1000} \times FieldWidth_0 \tag{3}$$

where z, denotes the depth in water. This correction is denoted as the simple edge correction. Additionally, we have considered another correction factor which takes into account the far edge of the field that is moving away from the SiPM probe. We generate this correction factor by integrating the intensity from the close edge of the beam to the far edge of the beam (assuming a non-diverging line of sight), this correction is denoted as the line integral correction.

Lateral scans are taken for 2 $\times$ 2 cm and 3 $\times$ 3 cm 6 MV fields at 100 cm source to axis distance (isocenter) with a water depth of 10 cm, as shown in Fig. 8. Since the distance between the edge of the field and the collimator remains constant during the lateral scan, a beam divergence correction factor is not necessary here (as opposed to PDD measurements where the field-edge and collimator distances both change with depth).

In order to quantify the spatial resolution of the probe, an edge spread function (ESF) is generated by blacking out a portion of the water tank and performing a lateral scan across the interface between the uncovered and blacked out regions of the water tank, as seen schematically in the top of Fig. 9. This resolution is heavily dependent on the geometry of the collimator and probe, which determines the solid angle of acceptance, as well as the distance from the collimator surface and axial width of the field (field size dependence). The ESF is generated under the same conditions as the PDD as well as the 3 $\times$ 3 cm lateral scan, and thus is only valid for those conditions. To determine the line spread function (LSF), the ESF points are interpolated (to generate more data points) using a spline function and is numerically differentiated. The modulation transfers function (MTF) is generated from the Fourier transform of the LSF (which is shown in Fig. 13 in the Results and Discussion sections).

Next, the ability to measure gradients in the radiation field by discerning changes in CE intensity during each Linac pulse is assessed. A small rectangular field size of 0.5 $\times$ 1 cm is used, where the 0.5 cm is the width of the field from the SiPM probe perspective. For this particular set of measurements, the probe was placed directly onto the surface of the tank with no collimator. A gradient is introduced by using 60° and 30° physical wedges which are subsequently attached to

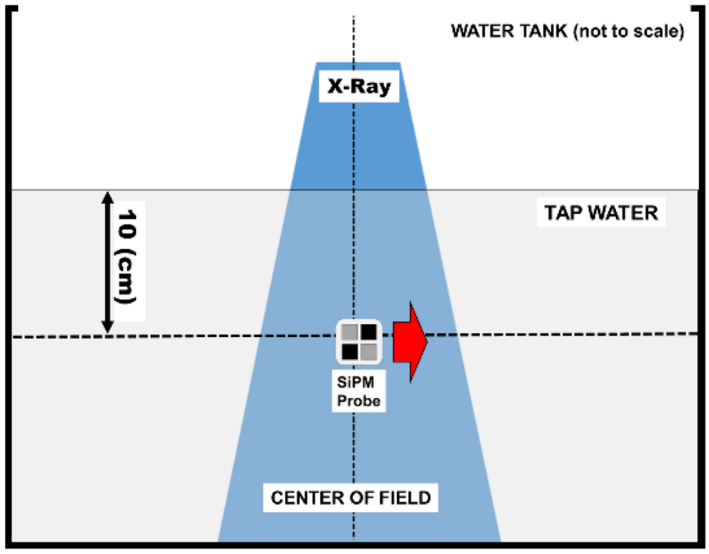

Fig. 8. Schematic of the lateral scan setup with the collimator facing into the Figure with the light collecting pixel aligned to the center of the field.

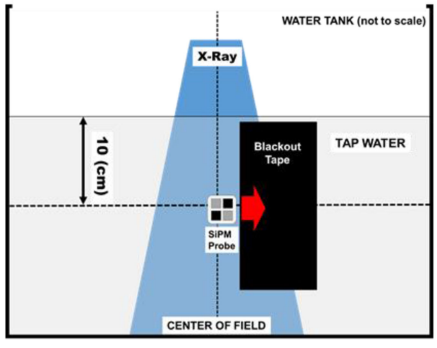

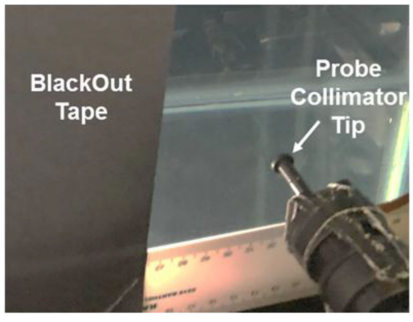

Fig. 9. Top: A schematic of the SiPM probe scanning across a blacked-out edge to measure the edge spread function. Bottom: A photograph of the blackout tape that is attached to the water tank.

the head of the Linac. The optical phantom consists of a water tank filled with municipal tap water. As shown schematically in Fig. 10, the center of the SiPM optical probe is attached to the outside of the tank and is aligned at 100 cm source-to-axis distance (SAD) with a water depth of 10 cm, corresponding to 90 cm source-to-surface distance (SSD). The field is then scanned across the wedge in a “step and shoot” fashion by adjusting the collimator jaw positions asymmetrically on the Linac. The probe position and the field stay fixed with respect to each other by adjusting the treatment couch position to move the relative probe position; since the water tank is perturbed due

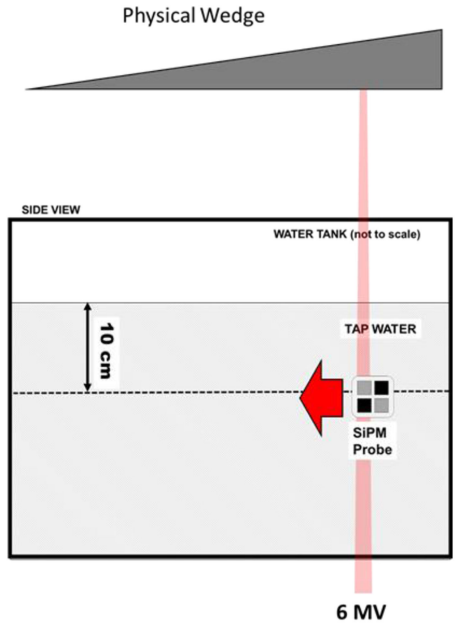

Fig. 10. Side view of the experimental setup. The probes are aligned so they are at a constant depth from the water surface (10 cm); a 0.5 $\times$ 1 cm 6 MV field is scanned across the physical wedge (30° and 60°) while the SiPM probe is repositioned to track the field.

to couch movement, the water is given 60 seconds to settle. Since measurements are taken along a gradient in the horizontal axis, the pixel adjacent and below to the open (light measuring) pixel is chosen to be the light-blocked pixel. This subtracts out any stem effect and stray radiation signals (which are on the order of 5% of the total signal collected from the open pixel) along the same point within the gradient.

Film dosimetry was used as a benchmark to compare the CE measurements. Radiochromic film was sandwiched between blocks of water-equivalent plastic, with 10 cm of solid water on top of the film, which is placed at 100 cm SAD to simulate the experimental conditions used for CE measurements. For these measurements, the film was irradiated with 2 Gy along the beam central axis with a 15 $\times$ 15 cm 6 MV field.

2.3 SiPM/Photodiode Comparison in Tissue

A photodiode (PD) system is used as a benchmark comparison for the SiPM probe, which consists of a commercial mounted silicon photodiode (Thorlabs SM05PD3A), DC Bias Module (Thorlabs PBM42), and a transimpedance amplifier (Texas Instruments OPA659) adjusted to have the same nominal amplification as that used for the SiPM probes (2200 V/A). The signal is acquired using the same oscilloscope (GW Instek GDS-3504) as for the SiPM Probes.

To simulate a soft tissue scenario, a phantom consisting of ground pork with a fat content of 12.4 vol% is used since it has both muscle and fat making it useful as a generic tissue phantom representing breast, head and neck, and tumor tissue types. Ground pork is placed into a 10 $\times$ 10 $\times$ 10 cm black painted acrylic box (with a thickness of 3 mm) and shaped to the geometry of the box. The top of the box is open with the ground pork flattened at the same level as the box, as seen on the top of Fig. 8. A clear polyethylene wrap (Saran wrap) is wrapped around the probe to act as a protective barrier between the SiPM/photodiode probe that is placed on top of the ground pork phantom. The photodiode probe itself has a limited acceptance solid angle (0.7π steradians) due to the geometry of the photodiode mounting. In order to make the SiPM comparable, a holder was made to reduce the acceptance solid angle of the SiPM probe from 2π to (0.7 $\pm$ 0.1) π steradians.

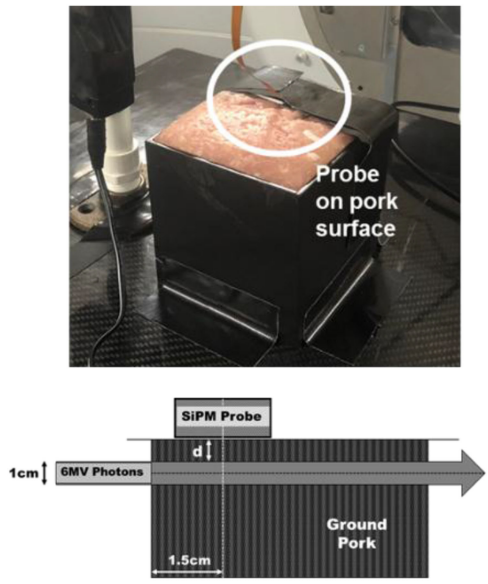

Fig. 11. **Top:** A photo of the experimental setup. **Bottom:** a schematic of the ground pork phantom. "d" is the distance between the edge of the pork phantom and the distance between the center of the probe and the edge of the phantom is 1.5 cm.

The bottom panel of Fig. 11 shows a schematic of the experimental setup. CE from a 1 $\times$ 3 cm 6 MV field is measured at various depths in the ground pork phantom, which is varied by adjusting the height of the treatment couch. Depth, d, is defined as the distance from the top edge of the field to the SiPM/PD. The probes are placed at a distance of 100 cm SAD, positioned 1.5 cm from the entrance side of the radiation field for maximum buildup of radiation dose. Measurements taken with black-out cloth material wrapped around the probes are subtracted from the overall measured signals at each depth to account for any CE originating from the polyethylene food wrap.

3. Results and Discussion

3.1 CE Dosimetry in Water Using the SiPM Probe

The top of Fig. 12 shows the measured lateral profile over an opaque edge. Over the opaque region, there is still a non-zero signal (0.05 V), this is from a background overall glow due to scattered CE in the water tank. The bottom of Fig. 12 shows the derived modulation transfer function and line spread function. The system spatial resolution, which is the full width half maximum (FWHM) of the line spread function, is 3.5 mm. Spatial resolution is a function of the collimator dimension and the spatial sampling interval. With a narrower collimator (keeping the length constant), the solid angle of detection can be reduced. Combined with finer spatial sampling intervals, a higher resolution can be obtained, though at the cost of lower signal strength, which can be offset with the higher sensitivity of the SiPM. On the other hand, imaging-based detectors (such as CCDs) are capable of finer resolution, but have lower signal gain, thus limiting CE measurements to superficial depths.

Lateral scans of 3 $\times$ 3 cm and 2 $\times$ 2 cm 6 MV fields are shown in Fig. 13. Compared with calculated lateral scans from the treatment planning system (TPS), the penumbra is more pronounced, never falling to zero in the same scan range (i.e., reduced contrast). This is from a combination of aperture effects from the collimator (the probe is integrating over a solid angle), as well as scattered background optical photons.

The top panel of Fig. 14 shows a comparison between the normalized CE intensity, measured using the SiPM probe, and the percent depth dose (PDD) ion chamber measurements in water

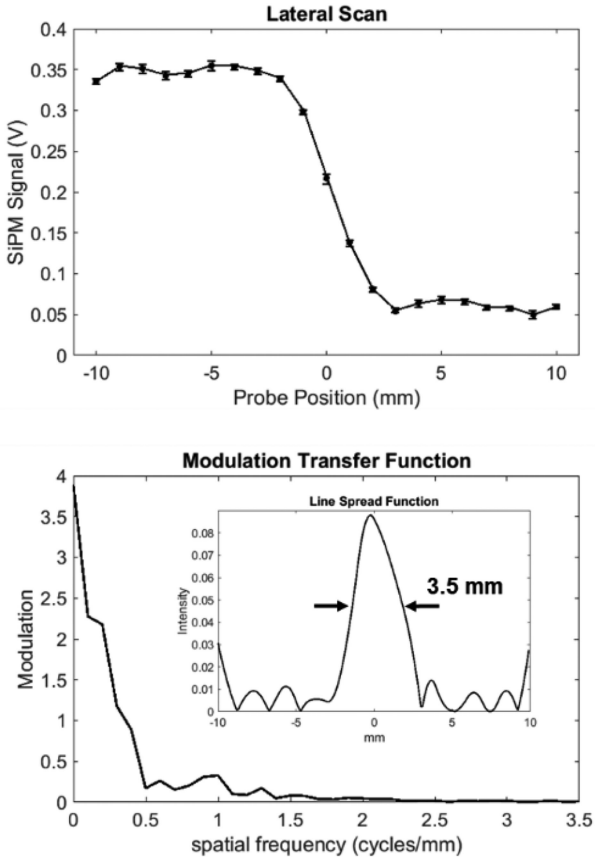

Fig. 12. Top: Lateral scan data across an optically opaque edge to generate an edge-spread function. Bottom: Using the edge-spread function above, the derived modulation transfer function; inset: derived line-spread function.

during the commissioning of the same Linac used in our experiments. Qualitatively, the data from the SiPM does show a build-up region followed by a fall-off region, as expected from a MV photon field. In the fall-off region, the SiPM probe is clearly overestimating the PDD; this is partly due to the geometry of the radiation beam: as it diverges, a correction factor must be used to take into account the change in distance between the edge of the field and the SiPM probe (as shown earlier in Fig. 7). This simple edge correction takes into account for such geometric effects in the effective point of measurement of the SiPM probe (see Section 2.2 above –Equation 1). Using this correction factor, the fall-off region of the SiPM probe is now closer to what is obtained from ion chamber measurements, as shown by the red dashed line in Fig. 15. The residual standard deviation between the simple edge-corrected SiPM CE intensity and the ion chamber PDD measurements (see Fig. 15, lower panel) is 2.4%. When considering that the edge furthest from the SiPM probe, the line integral correction is applied (see Section 2.2 above). This results in a SiPM PDD (blue dashed line in Fig. 15) that didn't agree as well with the ionization chamber PDD compared to the simple edge correction factor, which is subsequently adopted herein. Incidentally, previous work [11] has shown, using a CCD camera to image the relative CE intensity, that the PDD was underestimated by the CE in the fall-off region.

Fig. 15 shows CE intensity measured using the SiPM probe as a function of position for 30° and 60° physical wedges. A linear regression is used to determine the slope of each wedge measurement. For the 30° wedge, the slope (in arbitrary units per mm) is -1.386×10^{-3} ($R2 = 0.9496$) and -4.882×10^{-3} ($R2 = 0.9951$) for the 60° wedge, showing a steeper slope for the 60° wedge.

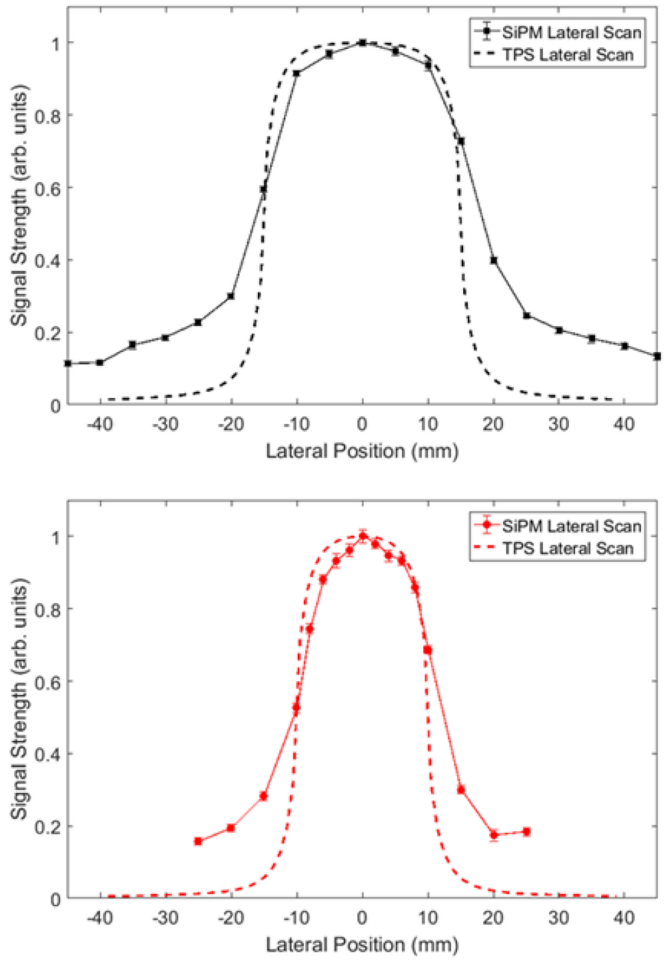

Fig. 13. Lateral scans of (top) 3 × 3 cm and (bottom) 2 × 2 cm 6 MV photon fields with the respective calculated scans using treatment planning software (dashed lines).

Radiochromic film measurements were again used as a comparison. The center of the film was normalized to arbitrary units and compared with the CE measurements. Qualitatively, the CE measurements match with the film measurements (i.e., the slopes are steeper for the 60° wedge vs the 30° wedge). There is deviation between the slopes of the film measurements, -2.389×10^{-3} *vs* -1.386×10^{-3} (a ratio of 1.72) and -6.360×10^{-3} *vs* -4.882×10^{-3} (a ratio of 1.30) for the 30° and 60° wedge, respectively. However, although the trends are consistent, there are deviations that can be attributed to two sources. The first and most prominent source is that the measurements with the SiPM probe are taken with an aperture averaging technique. From the perspective of the probe, the field is 0.5 cm; since there is a physical wedge, the output signal from the probe is the integration of the signal over that gradient. The other source of deviation may be due to slightly different film measurement conditions compared to the CE measurements. Film measurements were taken using a continuous field whereas the probe measurements are taken at discrete points.

3.2 SiPM/Photodiode Comparison in Soft Tissue

Table 1 shows the signal strength (in mV) for a both the SiPM and the photodiode (PD) at various ground pork depths, which is defined as the distance between the edge of the 6 MV 1 × 3 cm field and the probe surface (as shown in Fig. 11). As depth increases, the ratio of the SiPM-to-PD signal strength increases. After 5 mm, the PD signal is barely perceptible and after 7 mm of depth,

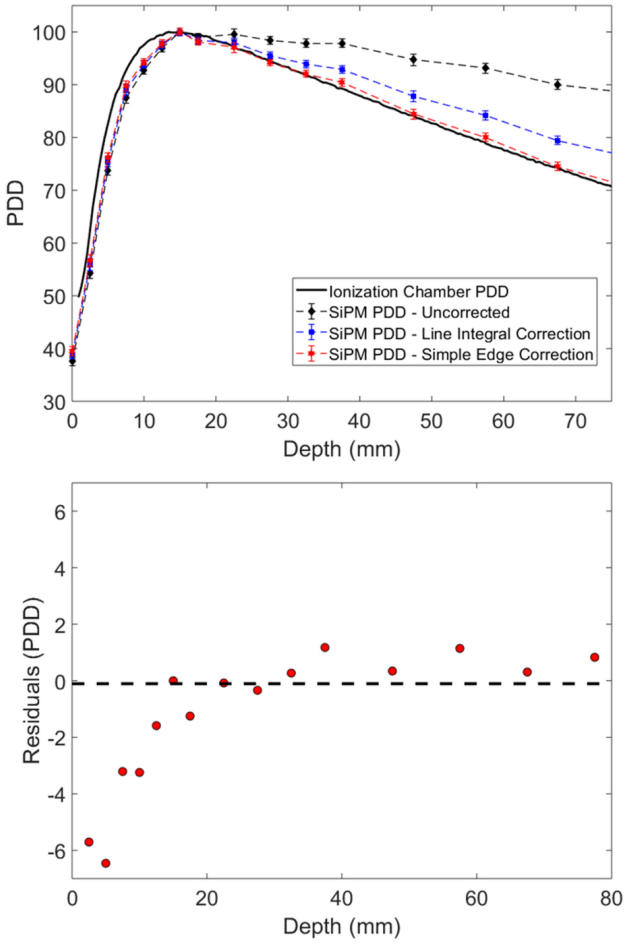

Fig. 14. Top: SiPM normalized signal strength (uncorrected, using a simple edge correction, and using a line integral correction) compared to the PDD measurements generated by scanning an ion chamber in a water tank for this Linac during its commissioning. Bottom: residuals [in units of percent depth dose] between the best corrected SiPM probe measured PDD data (simple edge corrected) and the expected values collected during Linac commissioning.

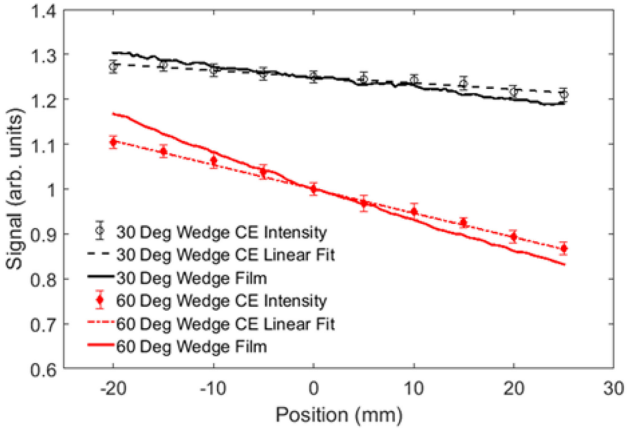

Fig. 15. Signals from the SiPM-based optical probe (dashed lines) corresponding CE from a 0.5 $\times$ 1 cm 6 MV photon field delivered by a Linac at different lateral positions with 30° and 60° wedges compared to corresponding radiochromic film measurements (solid lines).

TABLE 1

Signal Strength (mV) Versus the Depth (Defined As Distance Between the Probe and the Edge of a 1 × 3 cm 6 MV Field) in Ground Pork for Both the SiPM Probe and the Silicon PD Probe As Well As Their Relative Signal Strength (a Ratio of the SiPM and PD Values)

Depth (mm)	SiPM Signal (mV)	Photodiode Signal (mV)	Ratio (SiPM/PD)
1	944 ± 4	7.5 ± 0.2	126
5	490 ± 6	0.8 ± 0.1	612
7	364 ± 5	0.3 ± 0.1	1,213
35	24 ± 3	-	-

TABLE 2

A Qualitative Comparison Between Common Photodetector Technologies That Can Be Used for CE Measurements

	Compact Optical Probe Form Factor	Deep Tissue Optical Measurements	Superficial Tissue Optical Measurements
SiPM	***	***	***
(i)CCD/(i)CMOS	*	**	***
PMT	*	***	***
Si Photodiode	***	*	**

the signal is no longer detectable. However, at 35 mm depth, the SiPM is still acquiring a signal, hence, the SiPM probe can detect CE optical signals from radiation interaction that is at least five times deeper than what the PD probe can detect (35 mm vs. 7 mm). Beyond 35 mm, the SiPM is still acquiring a signal, however, this signal is no longer changing with depth, suggesting that subsequent signals are from an overall baseline signal from scattered photons, which is also seen as the baseline signal in the edge spread function measurements in Fig. 12 and is treated as background noise.

The peak of the CE is in the blue, which is outside of the biological optical window. In particular, absorption of blue light, for example by myoglobin in the ground pork phantoms employed here, leads to considerable weakening of the CE signal. Furthermore, current photodetector technologies such as photodiodes and CCDs are generally not as sensitive to blue light as other wavelengths. These factors present significant challenges for deep tissue CE measurements. On the other hand, the SiPM optical probe described here has distinct advantages over current detection methods such as photodiodes and CCDs, and thus constitutes an enabling step for using deep tissue CE for *in vivo* dosimetry by allowing for dose measurements deeper into the tissue than other optical imaging modalities.

For deep tissue optical measurements (>5 mm), every optical photon is valuable as only a small number of photons are escaping the tissue, this becomes particularly important if narrow spectral ranges are measured or if the signal lies outside of the biological window (where optical absorption from blood in tissue takes place). By placing an optical probe directly onto the skin, all optical photons leaving the tissue are collected, eliminating inverse square losses in intensity during standard imaging. For this application, SiPM-based optical probes are ideal. Silicon photodiodes also excel as optical probe sensors due to their form factor and work well for superficial tissue measurements (such as for pulse oximeters, [23]); however, for deep tissue CE measurements,

photodiodes lack such sensitivity, as demonstrated above. Intensified charge coupled devices (CCDs) and complementary metal oxide semiconductor (CMOS) devices offer excellent sensitivity but do not have the compact form factor of SiPMs/photodiodes (for example, most CCD cameras require active cooling to reduce thermal noise in low light application [24]), thus they must be placed at a distance away to image a region of interest, limiting their potential for deep tissue optical measurements (though they are excellent for superficial tissue optical measurements). Photomultiplier tubes (PMTs) also do not have a form factor that is congruent with compact optical probes, require a large bias voltage (∼1,100 V), and can accommodate a single channel only. Table 2 provides a qualitative summary of different optical devices and contrasts their application for CE. Future work will provide more quantitative analysis as these technologies become more mature in low photon counting applications such as CE.

4. Conclusion

While there are significant challenges with probing tissue which strongly scatters light, this work has shown the feasibility of using SiPMs as high-sensitivity optical sensors enabling novel deep-tissue applications of Cerenkov Emission (CE) during external beam radiotherapy (EBRT). In particular, our results demonstrate the superior performance of SiPMs in very low light conditions compared to silicon photodiodes, allowing for the detection of weak CE within tissue at depths approximately five times greater than existing technologies are capable of. This has important implications for achieving true *in-vivo* dosimetry and enabling real-time adaptive radiotherapy. In this context, our findings are a key demonstration that it is possible to obtain real-time quantitative treatment guidance, specific to the actual treatment volume. Future possibilities enabled by our approach are envisioned to take EBRT beyond conventional anatomical and functional guidance to include biological and molecular signatures encoded in the deep-tissue optical response of normal and cancerous tissue to CE, as will be reported in a forthcoming publication.

Acknowledgment

The authors would like to thank the technical staff at Endectra, LLC.

References

[1] R.S.N.A, *Introduction to Cancer Therapy (Radiation Oncology)*. (2017). [Online]. Available: https://www.radiologyinfo.org/en/pdf/intro_onco.pdf
[2] J. Axelsson, S. C. Davis, D. J. Gladstone, and B. W. Pogue, "Cerenkov emission induced by external beam radiation stimulates molecular fluorescence," *Med Phys.*, vol. 38, no. 7, pp. 4127–4132, 2011.
[3] J. L. Demers, S. C. Davis, R. Zhang, D. J. Gladstone, and B. W. Pogue, "Cerenkov excited fluorescence tomography using external beam radiation," *Opt Lett.*, vol. 38, no. 8, pp. 1364–1366, 2013.
[4] A. K. Glaser, W. H. A. Voigt, S. C. Davis, R. Zhang, D. J. Gladstone, and B. W. Pogue, "Three-dimensional Cerenkov tomography of energy deposition from ionizing radiation beams," *Opt Lett*, vol. 38, no. 5, pp. 634–636, 2013.
[5] R. Zhang, C. J. Fox, A. K. Glaser, and D. J. Gladstone, "Superficial dosimetry imaging of Cerenkov emission in electron beam radiotherapy of phantoms," *Phys. Med. Biol.*, vol. 58, no. 16, pp. 5477–5493, 2013.
[6] P. A. Čerenkov, "Visible radiation produced by electrons moving in a medium with velocities exceeding that of light," *Physical Rev.*, vol. 52, no. 4, pp. 378–379, 1937.
[7] L. V. Wang and H.-I. Wu, *Biomedical Optics: Principles and Imaging*, Hoboken, NJ, USA: Wiley-Interscience, 2007.
[8] S. L. Jacques, "Corrigendum: Optical properties of biological tissues: A review," *Phy. Med. Biol.*, vol. 58, no. 14, pp. 5007–5008, 2013.
[9] K. Tanha, A. M. Pashazadeh, and B. W. Pogue, "Review of biomedical Cerenkov luminescence imaging applications," *Biomed. Opt. Express*, vol. 6, no. 8, pp. 3053–65, 2015.
[10] R. Zhang, A. K. Glaser, D. J. Gladstone, C. J. Fox, and B. W. Pogue, "Superficial dosimetry imaging based on Cerenkov emission for external beam radiotherapy with megavoltage X-ray beam," *Med Phys.*, vol. 40, no. 10, p. 101914, 2013.
[11] A. K. Glaser, S. C. Davis, W. H. A. Voigt, R. Zhang, B. W. Pogue, and D. J. Gladstone, "Projection imaging of photon beams by the Cerenkov effect," *Med. Phys.*, vol. 40, no. 1, p. 012101, 2013.
[12] Z. Rongxiao, J. Andreozzi, D. J. Gladstone, W. H. Beeler, "Cherenkoscopy based patient positioning validation and movement tracking during post-lumpectomy whole breast radiation therapy," *Phys. Med. Biol.*, vol. 60, no. 1, p. L1, 2015.
[13] SensL, "An introduction to the Silicon photomultiplier," SensL, Cork, Ireland, Technical Note, 2011.

[14] B. Carmen, V. Stefaan, and H. Roel Van, "Evaluation of a compact, high-resolution SPECT detector based on digital silicon photomultipliers," *Phys. Med. Biol.*, vol. 59, no. 23, pp. 7521–7539, 2014.
[15] H. Zhang, R. Zhou, and C. Yang, "A PET detector module with monolithic crystal, single end readout, SiPM array and high depth-of-interaction resolution," *J. Instrum.*, vol. 11, no. 08, p. P08020, 2016.
[16] A. Mora *et al.*, "Fast silicon photomultiplier improves signal harvesting and reduces complexity in time-domain diffuse optics," *Opt. Express*, vol. 23, pp. 13937–13946, 2015.
[17] G. Maira, M. Mazzillo, S. Libertino, G. Fallica, and S. Lombardo, "Crucial aspects for the use of silicon photomultiplier devices in continuous wave functional near-infrared spectroscopy," *Biomed. Opt. Express*, vol. 9, pp. 4679–4688, 2018.
[18] E. Ferocino, E. Martinenghi, A. D. Mora, A. Pifferi, R. Cubeddu, and P. Taroni, "High throughput detection chain for time domain optical mammography," *Biomed. Opt. Express*, vol. 9, pp. 755–770, 2018.
[19] E. Ciarrocchi *et al.*, "Cherenkov luminescence measurements with digital silicon photomultipliers: A feasibility study," *EJNMMI Phys.*, vol. 2, no. 1, p. 32, 2015.
[20] J. Klein, D. Yankelevich, M. Judenhofer, D. Stephens, G. Mitchell, and S. Cherry, "The potential for higher spatial resolution using ultrasound-modulation of Cerenkov luminescence," *J. Nuclear Med.*, vol. 57, p. 591, 2016.
[21] L. M. Moutinho *et al.*, "Brachytherapy dosimeter with silicon photomultipliers," *Nucl. Instruments Methods Phys. Res. Section A: Accelerators, Spectrometers, Detectors Associated Equip.* vol. 787, pp. 358–360, 2015.
[22] R. Weissleder, "A clearer vision for in vivo imaging," *Nature Biotechnology*, vol. 19, pp. 316–317, 2001.
[23] J. Sinex, "Pulse oximetry: Principles and limitations," *American J. Emergency Med.*, vol. 11, no. 1, pp. 59–66, 1999.
[24] Andor, Sensitivity of CCD Cameras, Andor Application Note, Oxford Instruments. [Online]. Available: https://andor.oxinst.com/learning/view/article/sensitivity-of-ccd-cameras